2007 IEEE International Conference on
Robotics and Automation
Roma, Italy, 10-14 April 2007

Analysis of Circular Robot Jumping by Body Deformation

Yoshinari Matsuyama and Shinichi Hirai

Abstract— **As jumping is an effective method of moving over rough terrain, there is much interest in building robots that can jump, and deformation of a soft robot's body is an effective method to induce jumping. Our aim was to investigate the effect of the initial shape of deformation of a circular shell made of spring metal. Four initial shapes of deformation, dish, peanut, cup and cap, jumped the highest in that order, with the dish jumping twice as high as the cap. A simulation of a model was in good agreement with the observations.**

I. INTRODUCTION

Jumping is used ubiquitously by animals and insects as a means of locomotion because it is a very effective way of maneuvering, especially over obstacles. For this reason, engineers are keen to develop good jumping mechanisms for robots. Good progress has been made using soft actuators made from shape memory alloy (SMA), polymer or gel [1], [2], [3], [4], [5]. These actuators have the advantages of being light and soft, but most of them cannot generate an impulse, that is, an energy burst, large enough for jumping, and those that can require a wet environment or a high voltage, making it difficult to build self-supporting robots.

The actuators can make a soft object jump by deforming it, imparting potential energy. The object jumps if enough potential energy is released in a burst as the object returns back to its original shape. The aim of the present study was to improve the jumping capability of a soft robot. We investigated the jumping of a circular object by physical simulation and experiments. Section II describes the principle by which the objects jump by deformation. Section III presents experiments on how the initial shapes affect jumping. Section IV presents a simulation of the jumping. Finally, we describe the impulse of a circular robot as it jumps.

RELATED WORK

Hopping legged robots that can perform dynamic maneuvers over the ground [6], [7], [8], pendulum-type jumping machines that use a swing motion [9], and robots that can jump from a stationary state by using pneumatic actuators have been studied [10].

II. JUMPING SOFT ROBOT

Consider a robot that is circular at rest on the ground, as in Figure 1-(a). When it is deformed, as in Figure 1-(b), it is in a state of high potential energy. If the potential energy is released rapidly enough as the object recovers its resting shape, the robot will jump, as in Figure 1-(c).

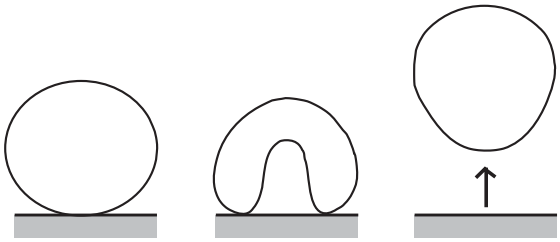

(a) natural shape (b) high-energy shape (c) jump

Fig. 1. Principle of jumping by deformation

Fig. 2. Jumping soft robot

Now let us consider a jumping robot that has already been studied [11]. The robot, which is shown in Figure 2, is soft and spherical. It consists of three circular shells made of spring metal arranged orthogonally to one another, and has 22 SMA coil internal actuators. By applying an appropriate voltage pattern to the coils, the robot can be made to jump as shown by the images in Figure 3, which were captured by a high-speed camera at 500 fps. Figure 3-(a) shows the body deformed, and thus with much potential energy. Releasing the stored potential energy rapidly makes the robot jump, as shown in Figure 3-(b) through Figure 3-(d).

III. JUMPING FROM DIFFERENT INITIAL DEFORMATION SHAPES

We investigate which of the four initial deformation shapes, shown in Figure 4, of a deformable robot that is circular at rest, produces the highest jump. The robot's body is made of spring metal and is 100 mm in diameter, 12 mm in width, and 0.15 mm in thickness, and weighs 4.6 g. The four shapes are created by securing parts of the body by the ends of threads crossing each other at a single point. We make the body jump by burning through all the threads at once at the crossing point, which suddenly allows the body to return

Y.Matsuyama is with Department of Robotics, Ritsumeikan University, Japan rr009021@se.ritsumei.ac.jp
S.Hirai is with Department of Robotics, Ritsumeikan University, Japan, hirai@se.ritsumei.ac.jp

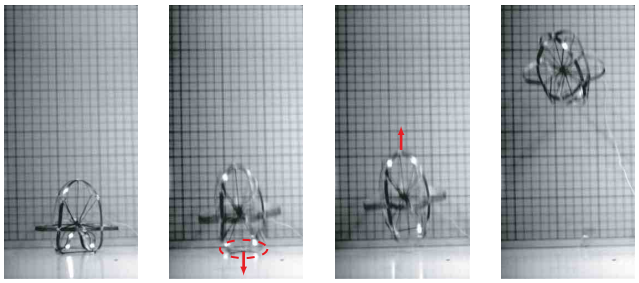

(a) 0 ms (b) 68 ms (c) 72 ms (d) 118 ms

Fig. 3. Successive images of soft robot jumping

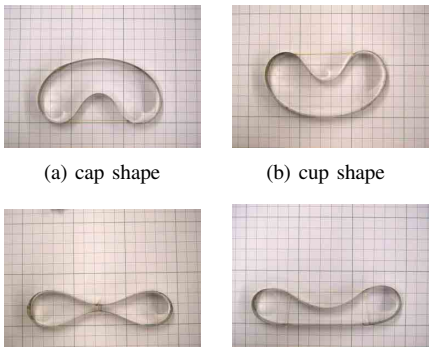

(a) cap shape (b) cup shape

(c) peanut shape (d) dish shape

Fig. 4. Initial deformation shapes tested for jumping capability

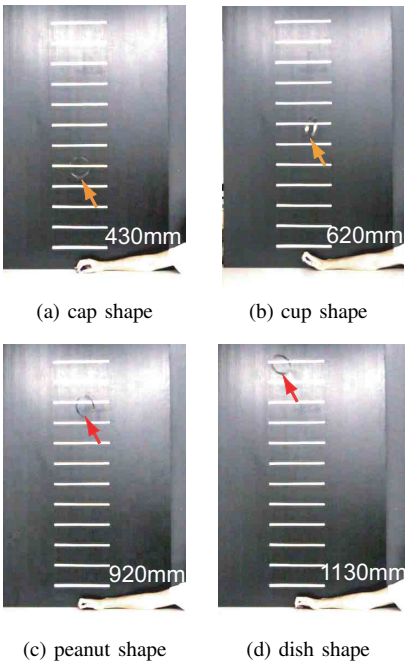

(a) cap shape (b) cup shape

(c) peanut shape (d) dish shape

Fig. 5. Effect of initial shape of deformation on jumping

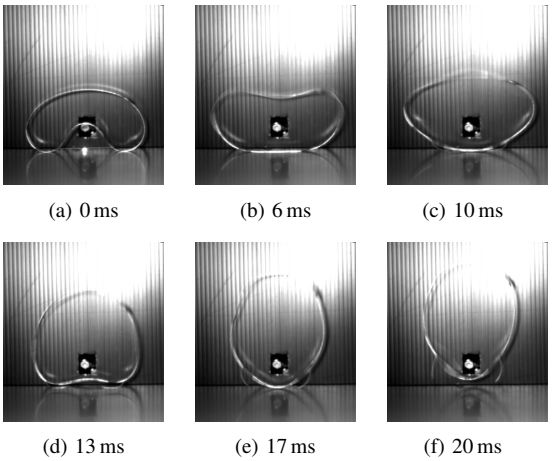

(a) 0 ms (b) 6 ms (c) 10 ms

(d) 13 ms (e) 17 ms (f) 20 ms

Fig. 6. Successive images of the cap shape jumping

to its stable shape. The cap shape in Figure 4-(a) is initially in contact with the ground only at a point on each side, and jumps when the central concave part strikes the ground. The cup shape in Figure 4-(b) is in contact with the ground at a point around the central convex part, and jumps when the concave part on the upper surface moves upward. The peanut shape in Figure 4-(c) has two concave parts, a lower and an upper, and jumps when the lower one hits the ground while the upper one moves upward. The dish shape in Figure 4-(d) has an area in contact with the ground, and jumps when the concave part on its upper surface moves upward. All four shapes have the same flexural potential energy, $U_{\text{flex}} = 16.0 \times 10^{-2}\,\text{Nm}$.

Figure 5 shows how each shape jumps. The arrows indicate the bottom of the objects in their highest positions and the value indicates the height of the bottom point. As you can see, the dish jumps the highest, followed in decreasing order, by the peanut, cup, and cap. Clearly, the jumping ability depends on the initial shape of deformation.

Figure 6 through 9 show successive images, captured by a high-speed camera at 1000 fps, of the objects jumping. Figure 6 shows the cap shape. The part that was initially concave hits the ground at 6 ms, and the sides that were initially touching the ground are no longer in contact at 10 ms and contact the ground again at 14 ms. The body jumps off the ground at 17 ms. Figure 7 shows the cup shape. The body turns into a cap shape at 4 ms, and jumps off the ground at 12 ms. Figure 8 shows the peanut shape. The part that was initially the top of the lower concavity collides with the ground at 3 ms. The body continues moving upward, and jumps off the ground at 12 ms. Figure 8 shows the dish shape. The bottom of the circular body remains in contact with the ground until the body jumps off the ground at 13 ms. Note that its area of contact decreases before jumping, and is very small immediately before the body leaves the ground.

IV. ANALYSIS OF SIMULATION OF JUMPING

In this section, we use a particle-based model to simulate the jumps of the four initial shapes. The deformable robot is modeled by a set of particles connected by mechanical elements. We formulate a circular body's flexural potential energy and simulate its dynamic behavior, including how it impacts the ground. We wrote the main computer program

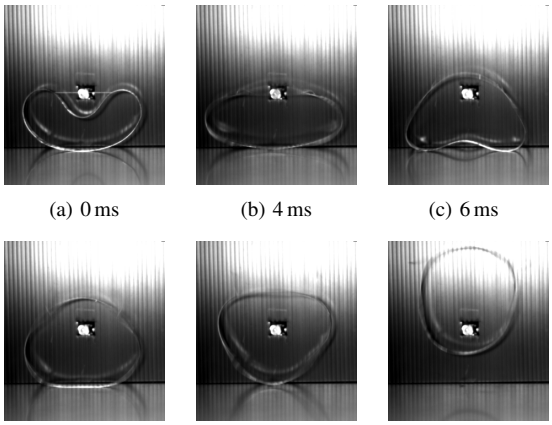

(a) 0 ms (b) 4 ms (c) 6 ms

(d) 9 ms (e) 12 ms (f) 20 ms

Fig. 7. Successive images of the cup shape jumping

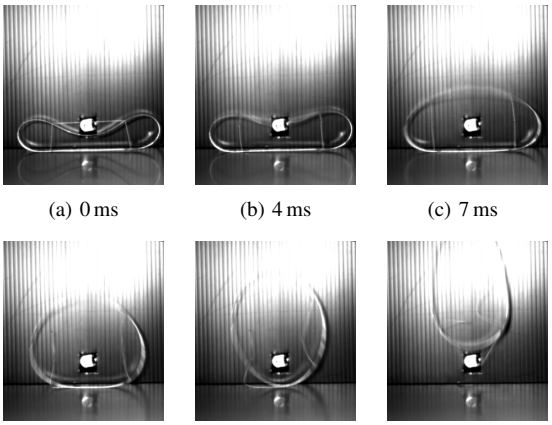

(a) 0 ms (b) 4 ms (c) 7 ms

(d) 10 ms (e) 13 ms (f) 20 ms

Fig. 9. Successive images of the dish shape jumping

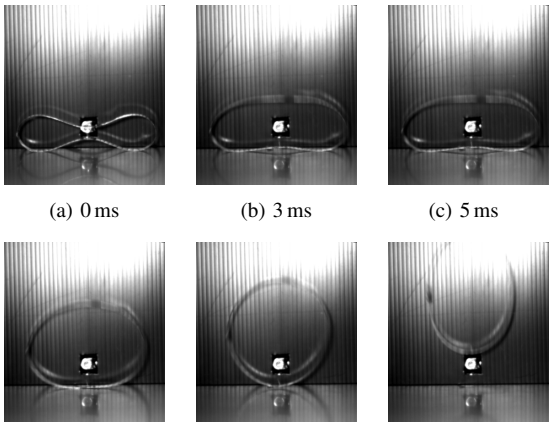

(a) 0 ms (b) 3 ms (c) 5 ms

(d) 9 ms (e) 12 ms (f) 20 ms

Fig. 8. Successive images of the peanut shape jumping

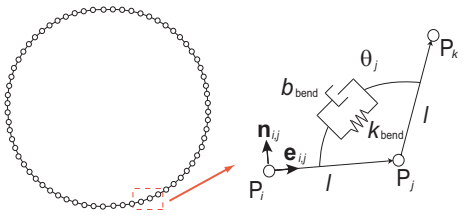

Fig. 10. Flexural Voigt model around shell particle

for the simulation in C/C++, and used OpenGL for the graphics display.

A. Flexural Potential Energy

Let us formulate the flexural potential energy of a circular body. Let L be the length of the circumference, P(s) is a point on the body at distance s from the origin point along the circumference, and $\theta(s)$ be the angle subtended by the tangent to P(s). The flexural potential energy of a circular robot can then be formulated as follows:

$$U_{\text{flex}} = \int_0^L \frac{1}{2} R_{\text{flex}} \left(\frac{\mathrm{d}\theta}{\mathrm{d}s} \right)^2 \mathrm{d}s, \tag{1}$$

where R_{flex} is the flexural rigidity at point P(s). We use the above equation to evaluate flexural potential energy of a circular body during dynamic simulation.

B. Particle-based Model of Circular Robot

Figure 10 shows the flexural Voigt model around a shell particle. P_i and P_k are the particles adjacent to P_j, separated by angle θ_j around particle P_j. Torque τ_j around particle P_j is then given by

$$\tau_j = k_{\text{bend}} \theta_j + b_{\text{bend}} \dot{\theta}_j, \tag{2}$$

where k_{bend} is the flexural elastic constant and b_{bend} is the flexural viscous constant. $\mathrm{e}_{i,j}$ is the unit vector along the edge from P_i to P_j and $\mathrm{n}_{i,j}$ is the unit vector perpendicular to vector $\mathrm{e}_{i,j}$. We assume that vectors $\mathrm{e}_{i,j}$ and $\mathrm{n}_{i,j}$ form a right-handed coordinate system. Distance l is fixed between two neighboring particles. Torque τ_j can be equivalently converted into three forces, $-(\tau_j/l)\mathrm{n}_{i,j}$ on P_i, $-(\tau_j/l)\mathrm{n}_{j,k}$ on P_k and $(\tau_j/l)\mathrm{n}_{i,j} + (\tau_j/l)\mathrm{n}_{j,k}$ on P_j.

C. Model of the Ground

Collision with the ground makes a circular robot jump. Let us model the ground to simulate the collision between a robot and the ground. Figure 11 shows a Voigt model of the ground. k_{ground} is the elastic coefficient and b_{ground} is the viscous coefficient. Particle P_j is assumed to be beneath the surface of the ground. A repulsive force f_{ground} is then applied to the particle. d_j is the depth to which particle P_j has penetrated the ground. The repulsive force can then be expressed as:

$$f_{\text{ground}} = k_{\text{ground}} d_j + b_{\text{ground}} \dot{d}_j. \tag{3}$$

Let μ be the coefficient of friction of the ground. Then, the force of friction on particle P_j is μf_{ground} .

D. Initial Shapes and Flexural Potential Energy

Figure 12 shows the initial deformed shapes of the actual circular body made of spring metal, while Figure 13 shows

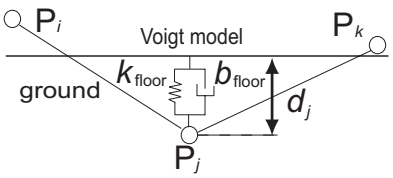

Fig. 11. Model of the ground

the shapes in a simulation model. From (1), the flexural potential energy of all the initial shapes is 4.37×10^{-2} Nm, since the flexural rigidity R_{flex} is 6.95×10^{-4} Nm^2, calculated from Young's modulus and the geometric moment of inertia of the spring steel. Figure 12-(a-1) through (a-3) show cap shapes. The shape in Figure 12-(a-1) has lower flexural potential energy than that in Figure 12-(a-3). Figure 12-(b-1) through (b-3) show cup shapes, Figure 12-(c-1) through (c-3) show peanut shapes, and Figure 12-(d-1) through (d-3) show dish shapes. For all the shapes in Figure 12-(a-1), (b-1), (c-1) and (d-1) $U_{\text{flex}} = 8.77 \times 10^{-2}$ Nm, while for all those in Figure 12-(a-2), (b-2), (c-2) and (d-2), $U_{\text{flex}} = 12.3 \times 10^{-2}$ Nm, and for all those in Figure 12-(a-3), (b-3), (c-3) and (d-3), $U_{\text{flex}} = 16.0 \times 10^{-2}$ Nm. Assume that the stored flexural energy is completely converted into the gravitational energy. Note that the jump height depends on the size of the difference in the flexural potential energy between the initial shapes and the stable circular shape.

E. Results of Jumping Simulation

Here, we model the 4.6 g circular shell as a series of 64 particles, weighing 0.071 g each. k_{bend} was measured as 0.1417 Nm/rad and b_{bend} as 0.00002 Nm/(rad/s). Assume that the ground is made of steel, then $k_{\text{ground}} = 1.0 \times 10^6$ N/m, and $b_{\text{ground}} = 1.0 \times 10^3$ Ns/m. Let the coefficient of kinetic friction be 0.3 and the coefficient of static friction be 0.5. Table I compares the jumping heights obtained from experiments and simulations. Note that the figures are the center of gravity at the highest point of each jumping. Recall that the flexural potential energy has the same value for all shapes shown in Figure 12-(a-3), (b-3), (c-3) and (d-3), but the cap in Figure-12(a-3) jumps 457 mm, while the dish shape in Figure 12-(d-3) jumps 1171 mm, more than double. The simulated and experimental results are in good agreement. The maximum error is 15.8 % in the case of the peanut shape in Figure12-(c-1). Figure 14 shows successive images of the cup shape, shown in Figure 13-(b-3), by the simulation. Comparison of the simulated results and the experimental results in Figure 7, the deformed shapes during jumping are in good agreement. Therefore, the simulation is appropriate.

F. Impulse from the Ground during Jumping

Let us investigate the reaction force and the impulse from the ground during the jumping process by simulations. Figure 15 shows the reaction force from the ground during jumping. Figure 15-(a) shows reaction forces during jump starting from the cap shapes given in Figure 12-(a-1) through (a-3). An impulsive large force is exerted when the bottom of the body collides with the ground. Figure 15-(b) shows reaction forces when the cup shapes in Figure 12-(b-1) through (b-3) jump. A large force is generated when the bottom of the body collides with the ground. The force acts for several milliseconds after the collision. Figure 15-(c) shows reaction forces when the peanut shapes in Figure 12-(c-1) through (c-3) jump. It generates a force for a longer time than do the cap shapes. Figure 15-(d) shows reaction forces when the dish shapes in Figure 12-(d-1) through (d-3) jump. No impulsive force is generated. A relatively small force is applied for a longer time, almost 15 ms. From the results, the maximum reaction force from the ground does not directly influence the height of the jump.

The impulses of the particles from the ground can be computed by integrating the force with respect to time. As shown in Figure 16-(a), the impulse of the cap shapes increases rapidly when the bottom part of the circular body collides with the ground. Then, the impulse of the cap shapes increases more slowly, until that reaches a plateau. As shown in Figure 16-(b), the impulse of the cup shapes increases quickly from about 7 ms, and then reaches a plateau. As shown in Figure 16-(c), the impulse increases monotonously after the body collides with the ground. As shown in Figure

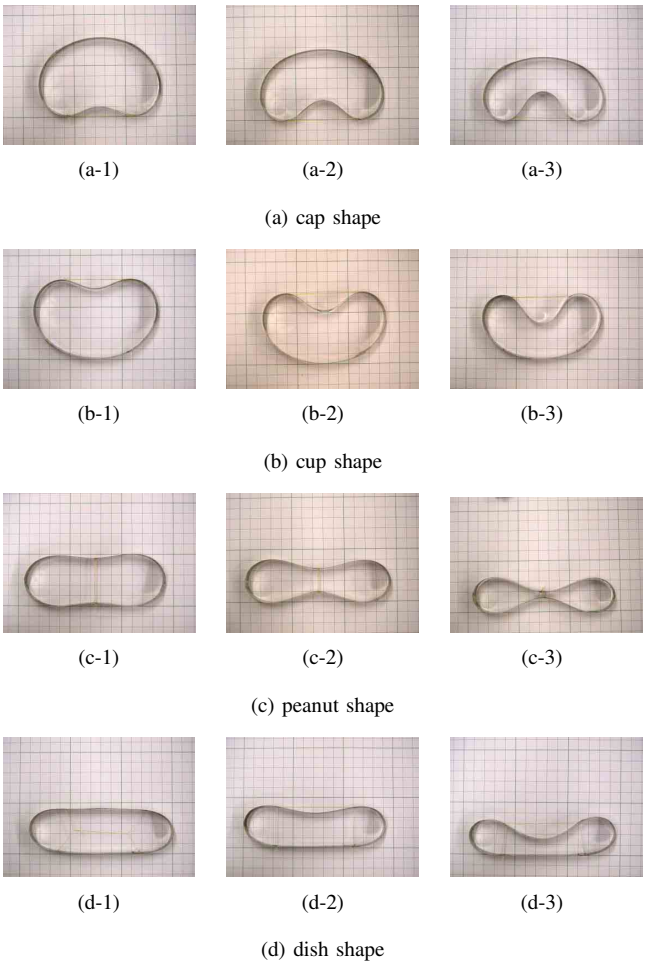

(a-1) (a-2) (a-3)

(a) cap shape

(b-1) (b-2) (b-3)

(b) cup shape

(c-1) (c-2) (c-3)

(c) peanut shape

(d-1) (d-2) (d-3)

(d) dish shape

Fig. 12. Initial shapes for jumping

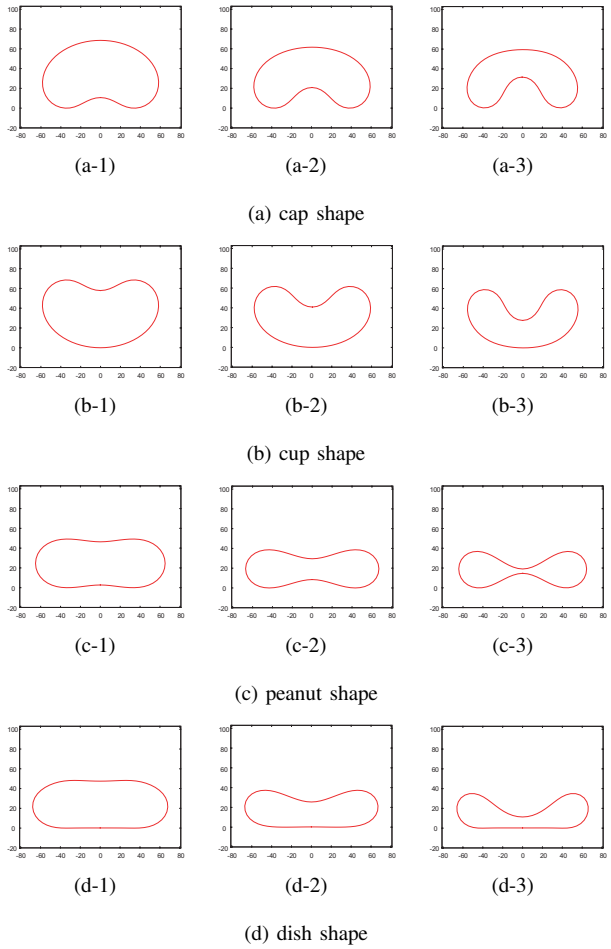

Fig. 13. Four initial shapes with different flexural potential energies

TABLE I

THE CENTER OF GRAVITY AT THE HIGHEST POINT

	experiment [mm]	simulation[mm]
cap shape		
(a-1)	270	271
(a-2)	410	382
(a-3)	480	457
cup shape		
(b-1)	260	272
(b-2)	490	483
(b-3)	670	669
peanut shape		
(c-1)	550	462
(c-2)	800	771
(c-3)	970	980
dish shape		
(d-1)	570	495
(d-2)	920	876
(d-3)	1180	1171

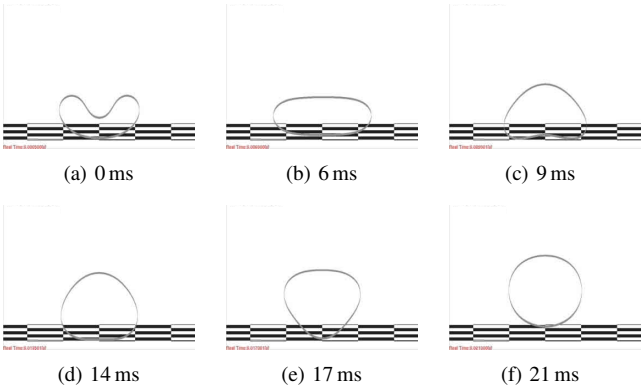

Fig. 14. Successive images of the cup shape jumping by simulation

16-(d), the impulse increases monotonously from the initial state. Note that when the stored flexural potential energy of the initial shapes is same, the maximum reaction force of dish shapes is the least in the four shapes. Surprisingly, the maximum impulse of dish shapes is the best one. Comparison of the Figure 12-(a-3), (b-3), (c-3) and (d-3), jump height is related to the maximum force of the impulse.

G. Energies of Circular Robot during Jumping

Figure 17 shows kinetic and potential energies of the circular robot jumping from the initial shapes in Figure 12-(a-3), (b-3), (c-3) and (d-3). Note that the chain double-dashed lines show the time when the body leaves the ground. The pie charts show the ratio of the each energy at the each time. Assume that the ratio of the total energy at 0 ms is 100 %. Figure 17-(a2), (b2), (c2) and (d2) shows the ratio at 5 ms. Figure 17-(a3), (b3), (c3) and (d3) shows the ratio at the time when the body leaves the ground. Figure 17-(a4), (b4), (c4) and (d4) shows the ratio at the time when the body is the highest point. In the initial shapes, the flexural potential energy occupies most area of the pie chart. After the restriction is removed, the flexural potential energy is converted into the kinetic energy. After the body jumps, the kinetic energy is converted into the gravitational energy. As shown in Figure 17-(a), the kinetic energy decreases when the bottom part collides with the ground. On the other hand, the kinetic energy increases, as shown in Figure 17-(d). Comparison of Figure 12-(a-3), (b-3), (c-3) and (d-3) shows that the energy loss of the dish shapes is the least. Table II shows the ratios to convert their flexural potential energy into gravitational energy during jumping. The ratio is 100 % when all the flexural potential energy is completely converted into the gravitational energy. From the table, we find that the stored flexural potential energy is wasted the most in the case of the cap shapes and used most efficiently in the case of the dish shapes.

V. CONCLUSION

We showed that the initial shape of deformation of a circular, soft body influences its jumping capability. Four initial shapes of deformation, dish, peanut, cup and cap, jumped the highest in that order, with the dish jumping twice as high as the cap. Next, we investigated the flexural potential energy of the deformed shapes, and then used a particle-based model to simulate the jumps made by the four shapes. The results agreed well with the observations. Finally, we examined the release of the stored potential energy, and

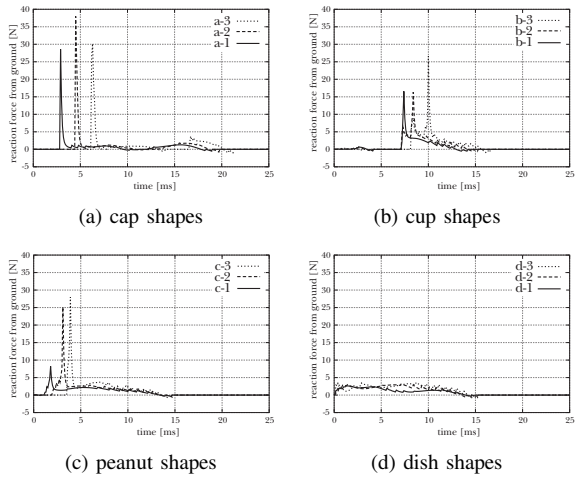

(a) cap shapes (b) cup shapes

(c) peanut shapes (d) dish shapes

Fig. 15. Reaction force from ground

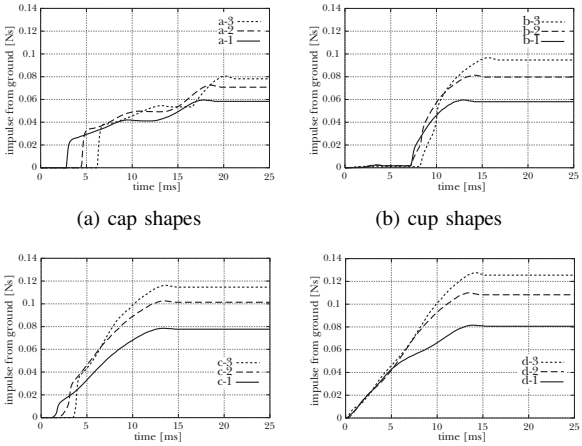

(a) cap shapes (b) cup shapes

(c) peanut shapes (d) dish shapes

Fig. 16. Impulse from ground during jumping

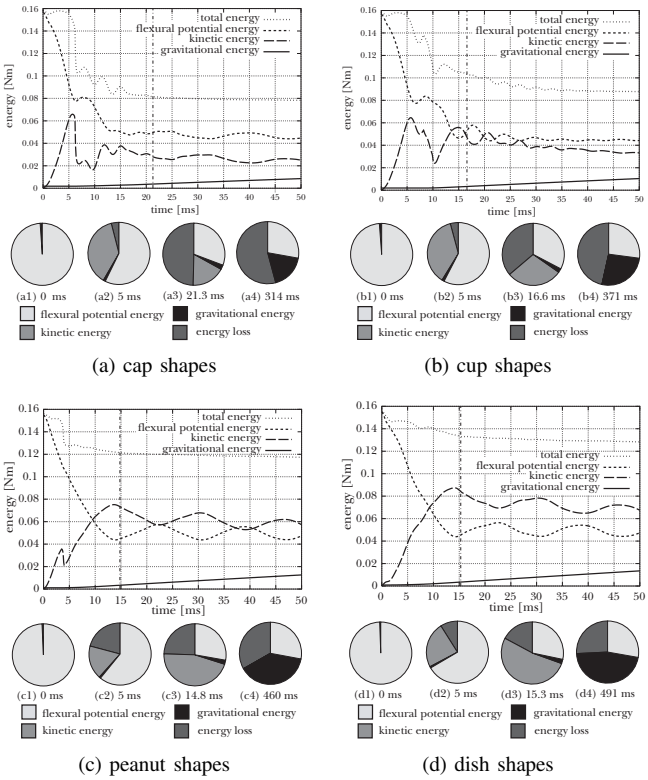

(a) cap shapes (b) cup shapes

(c) peanut shapes (d) dish shapes

Fig. 17. Kinetic and potential energies of a circular robot during jumping

TABLE II

CONVERSION OF FLEXURAL POTENTIAL ENERGY INTO GRAVITATIONAL ENERGY

	a	b	c	d
1 (8.77×10^{-2} Nm)	39.3 %	39.4 %	66.9 %	71.7 %
2 (12.3×10^{-2} Nm)	30.6 %	38.7 %	61.7 %	69.9 %
3 (16.0×10^{-2} Nm)	25.1 %	36.7 %	53.8 %	64.3 %

found that the jump height is related to the maximum force of the impulse. We found that the flexural potential energy stored in the circular body is wasted most in the case of the cap shape, and used most efficiently in the case of the dish shape.

We are going to apply our findings to a soft robot driven by soft actuators, and extend our study to a 3D model of the jumping process.

VI. ACKNOWLEDGMENT

This research was supported in part by the NEDO 21st Century Robot Challenge Program, Japan.

REFERENCES

[1] Pelrine, R., Kornbluh, R., Pei, Q., and Joseph, J., "High-speed Electrically Actuated Elastomers with Strain Greater Than 100%", *Science*, Vol. 287, February, pp.836–839, 2000.

[2] Ashley, S., "Artificial Muscles", *Scientific American*, October, pp.34–41, 2003.

[3] Hirai, T., Uddin, Z., Zheng, J., Yamaguchi, M., Kobayashi, S., Watanabe, M., and Shirai, H., "Quick and large electrostrictive deformation of non-ionic soft polymer materials", *Smart Structures and Materials 2003, Proc. SPIE*, Vol. 5051, pp.198–206, 2003.

[4] Choi, H. R., Jung, K. M., Kwak, J. W., Lee, S. W., Kim, H. M., Jeon, J. W., and Nam, J. D., "Digital Polymer Motor for Robotic Applications", *Proc. IEEE Int. Conf. on Control Applications*, Taipei, September, pp.1857–1862, 2003.

[5] Selden, B., Cho, K.-J., and Asada, H.-H., "Segmented Binary Control of Shape Memory Alloy Actuator Systems Using the Peltier Effect", *Proc. IEEE Int. Conf. on Control Applications*, New Orleans, April, pp.4931–4936, 2004.

[6] Raibert, M. H., "Legged Robots that Balance", *The MIT Press*, Cambridge, 1986.

[7] Hodgins, J. K. and Raibert, M. H., "Biped Gymnastics", *Int. J. of Robotics Research*, Vol. 9, No. 2, pp.115–132, 1990.

[8] Higashimori, M., Harada, M., Yuya, M., Ishii, I., and Kaneko, M., "Dimensional Analysis Based Design on Tracing Type Legged Robots", *Proc. IEEE Int. Conf. on Robotics and Automation*, pp.3744–3749, Barcelona, April, 2005.

[9] Hayashi, R., and Tsujio, S., "A Pendulum-type Jumping Machine Utilizing Human's Swing", *Journal of the Robotics Society of Japan*, Vol.19, No.4, pp.528-534, 2001.

[10] Kikuchi, F., Ota, Y., and Hirose, S., "Basic Performance Experiments for Jumping Quadruped", *Proc. IEEE Int. Conf. on Intelligent Robots and Systems*, Las Vegas, Nevada, October, 2003.

[11] Sugiyama, Y., and Hirai, S., "Crawling and Jumping by a Deformable Robot", *Int. J. of Robotics Research*, Vol.25, No.5-6, pp.603-620, May-June, 2006.